Proceedings of the Fifth IIEEJ International Workshop
on Image Electronics and Visual Computing 2017
Da Nang, Vietnam, February 28 - March 3, 2017

3D RECONSTRUCTION OF PANCREATIC DUCTS AND COLLAGEN FIBERS FROM PATHOLOGICAL IMAGES OF PANCREAS SERIAL SECTIONS

Hideki Komagata[*a], Masahiro Ishikawa[a], Kazuma Shinoda[b], Naoki Kobayashi[a],
Chika Iwamoto[c], Kenoki Ohuchida[d], Makoto Hashizume[c]
[a] Faculty of Health and Medical Care, Saitama Medical University,
1397-1 Yamane, Hidaka, Saitama, 350-1241, Japan;
[b] Graduate School of Engineering, Utsunomiya University,
7-1-2 Yoto, Utsunomiya, Tochigi, 321-8585, Japan;
[c] Department of Advanced Medical Initiatives, Faculty of Medical Sciences, Kyushu University,
3-1-1 Maidashi, Fukuoka Higashi-ku, Fukuoka, 812-8582, Japan;
[d] Department of Surgery and Oncology, Graduate School of Medical Sciences, Kyushu University,
3-1-1 Maidashi, Fukuoka Higashi-ku, Fukuoka, 812-8582, Japan

ABSTRACT

We will target the discovery of small lesions which CT (computed tomography) or MRI (magnetic resonance imaging) missed, and have studied registration of the 3-dimentional (3D) structure obtained by pathological images and the 3D structure obtained by CT or MRI. As previous step, we extracted pancreatic ducts and collagen fiber regions from HE (Hematoxylin and Eosin) stained pathological specimens of pancreas serial sections, and reconstructed of them. They consist of an image alignment between the different sections, a region extraction, and 3D reconstruction. The image alignment is used a template matching by a NCC (normalized cross-correlation) method. The region extraction of the collagen fiber is used machine learning by a SVM (support vector machine). As feature values for the SVM, we used image intensities, shape feature values, and texture feature values using co-occurrence and run-length matrix. The region extraction of the pancreatic ducts is used 3D labeling method, and the 3D reconstruction is used a volume rendering software.

1. INTRODUCTION

Histopathological diagnosis has been conducted to determine the presence or absence and type of lesion. It has primarily been carried out by slicing tissue sections taken by surgeries, staining them, and observing the slide with a microscope which is 2-dimensional (2D) histopathological image. In recent years, some study on 3-dimensional (3D) pathological analysis is conducted using pathological images of serial sections to obtain 3D morphological features which are such as volume of tumors and connectivity of structure [1][2][3]. On the other hand, the 3D structure analysis has been conducted for a long time in fields of CT (computed tomography) and MRI (magnetic resonance imaging). They are non-invasive, and intended primarily for early detection of lesions; however, it has a low resolution compared to the pathological image, and the discovery of small lesions is difficult.

We will target the discovery of small lesions that has been overlooked in conventional diagnoses of CT or MRI, and have studied about connection and modeling between the 3D structure obtained by pathological images and the 3D structure obtained by CT or MRI [4]. As previous step, we focus on the pancreas, and present extraction and 3D reconstruction methods of pancreatic ducts and collagen fiber regions from pathological specimens of pancreas serial sections.

In histopathological diagnoses, HE (Hematoxylin and Eosin) stain is frequently used to determine a variety of organizational structure. Hematoxylin stains cell nuclei and ribosomes in blue-violet. Eosin stains cell cytoplasm, red blood cells, and fibrous tissue in pink. We use therefore pathological images of the HE staining for 3D reconstruction. On the other hand, the structure recognition of collagen fibers are also used Masson's trichrome (MT) staining. We also use this MT staining for the recognition of collagen fibers.

2. MATERIALS AND METHODS

2.1. Materials

We used a KPC genetically modified mouse which follow the similar course to human pancreatic cancer. We administered the GEM (gemcitabine) 2 times a week to the 16-week-old KPC mouse, and acquired 3D MR images of the mouse once a week for observation of the temporal change. After the mouse died at 21-week-old, we were formalin-fixed immediately, extracted the pancreas, and acquired 3D MR and CT images of the pancreas. Next, we had 899 slices of the extracted

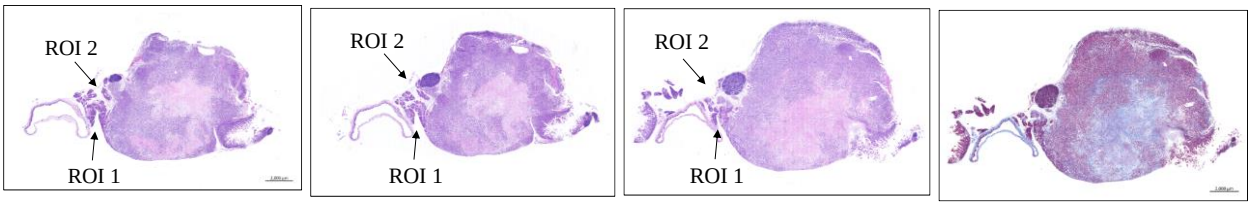

(a) 2nd slice, HE staining. (b) 55-th slice, HE staining. (c) 219-th slice, HE staining. (d) 220-th slice, MT staining

Figure 1. Whole slide images of pancreas serial sections stained HE and MT.

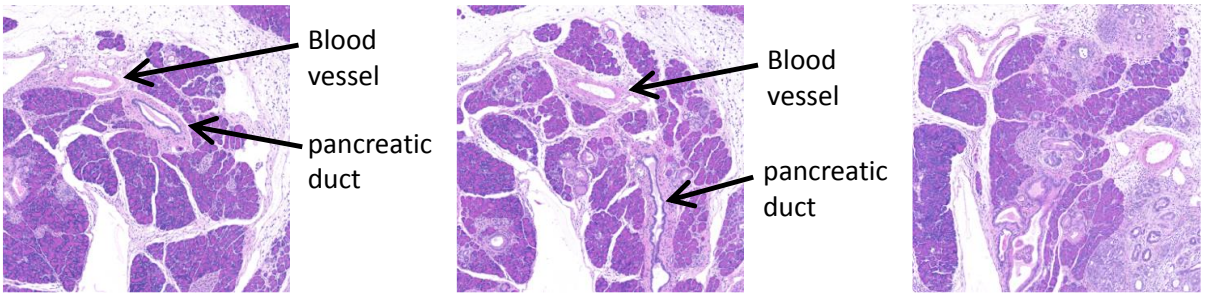

(a) 2nd slice, HE staining. (b) 55-th slice, HE staining. (c) 219-th slice, HE staining.

Figure 2. ROIs of Figure 1 (a) to (c).

pancreas in 4 μm interval, stained 809 slices of them with HE, and stained one slice of them with MT. In addition, we took their whole slide images in a virtual slide scanner at about 7 time magnification. Figure 1 (a), (b), and (c) show HE stained images of the 2nd slice, the 55-th slice, and the 219-th slice, respectively. Figure 1 (d) shows the MT stained image of the 220-th slice. The image size of Figure 1 (a) is 14,699 × 9,088 pixels.

2.2. Image registration and ROI extraction

Comparing Figure 1 (a) and (c), which are the 2nd and the 219-th slice images, there are variations in the position, size, and depth of staining of the tissue. These variations appear because to create a pathology specimen one by one. We therefore corrected them in the following procedure.

(1) Each tissue region was extracted in each slide image by binarization and hole filling. Threshold of the binarization was experientially 235 of Y value on YCbCr colorimetric system.
(2) 1st to 660-th slice images were enlarged so that extracted regions were same area. Images after 660-th slice were excluded, because their tissue regions were clearly smaller.
(3) Red, green, and blue (RGB) components on each image were gamma corrected so that average intensities of each component on each image were same intensity.
(4) Align the images in consideration of rotation and translation using a template matching. As an evaluation function model of the template matching, we used a normalized cross-correlation (NCC) model.

After these corrections, we manually clipped a region of interest (ROI) from 1st slice image where included pancreatic ducts and collagen fiber regions. ROIs of second and subsequent were automatically clipped using the template matching with NCC model. Some of the extracted ROIs are shown in Figure 2 (a) to (c). Their ROIs sizes are 1,000 × 1,000 pixels, and their ROIs positions are "ROI 1" in Figure 1.

2.3. Extraction of collagen fiber regions

2.3.1. Extraction overview

For extracting collagen fiber regions from ROIs obtained in Section 2.2, we used a support vector machine (SVM) [5][6] which is supervised machine learning, and identified whether each pixels on ROIs were the collagen fiber or not. The training data was manually created by filling a ROI of the HE stained image in reference to an enlarged image (Figure 3 (a)) of the MT staining image (Figure 1 (d)). Figure 3 (b) shows the ROI of the HE stained image before filling. Its slide number is 219 which is next to MT staining image (Figure 1 (d)), and the ROI size is 512 × 512 pixels.

Figure 3 (c) shows the training data which is the ROI after filling, and the red pixels on Figure 3 (c) are collagen fiber pixels (correct data for the machine learning of the SVM). The number of collagen fiber pixels on Figure 3 (c) is 22,384, whereas the number of non-collagen fiber pixels is 239,760, which is about 10

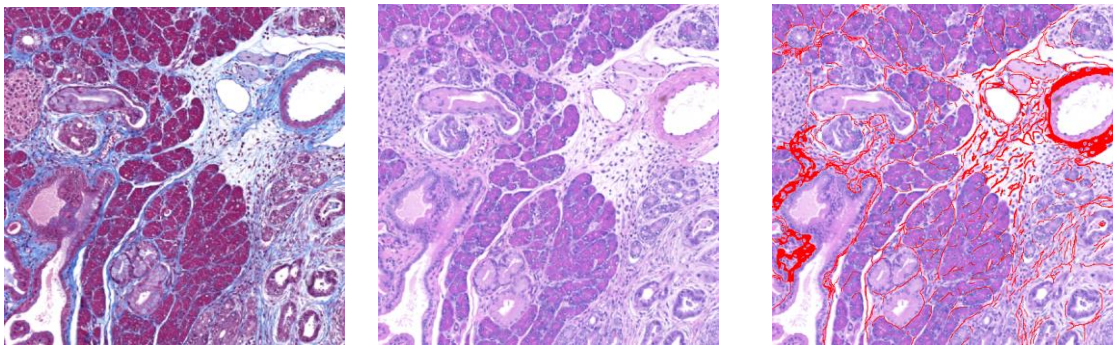

(a) 220-th slice, MT staining. (b) 219-th slice, HE staining. (c) Training data created by filling (b).

Figure 3. (a) and (b) is a reference image and an original image for creating a training data of a machine learning, respectively. (c) is the training data which was manually filled collagen fiber regions as red.

times greater than the number of collagen fiber pixels. In order to reduce the deviation of the learning result, it is better to make the number of input data uniform. We therefore randomly sampled non-collagen fiber pixels and provided them as input data for the machine learning.

As feature values for the SVM, we used RGB intensities of each pixels on ROIs, shape feature values described in Section 2.3.2, and texture feature values described in Section 2.3.3. The details of the SVM parameters are described in Section 2.3.4.

2.3.2. Shape feature values

For calculation shape feature values, we created binary images used by thresholds of intensities 160, 170, 180, 190, 200, 210, 220, and 230 of each RGB components on ROIs, extracted their labels by using a labeling algorithm, and calculated areas and circularities of labels. The obtained values were applied to each pixel on the label. If pixels on ROIs were not on extracted labels, their areas and circularities values were applied both 0. The total number of shape features is 48, because 8 thresholds, 3 color components, and 2 types of features were used.

2.3.3. Texture feature values

As texture feature values, we used 13 Haralick features (Energy, Correlation, Contrast, Sum Average, Variance, Sum Variance, Difference Variance, Entropy, Sum Entropy, Difference Entropy, Inverse Difference Moment, Information Measures of Correlation 1, and Information Measures of Correlation 2) [7] and 5 Run-length features (SRE, LRE, GLN, RLN, and RP) [8]. These are derived from a gray-level co-occurrence matrix (GLCM) and a gray-level run-length matrix (GLRLM).

Their input data was given by intensities of each RGB components in regions of 7 × 7 pixels and 21 × 21 pixels centered on the target pixel. Calculations angles of GLCM and GLRLM were used 0, 45, 90, and 135 degrees, and means of features calculated from their matrix were used as texture feature values. Furthermore, we used 1 pixel as an inter pixel distance (IPD) for the GLCM, and quantized ROIs into 64 gray levels before calculation of GLRLM. The total number of texture features is 108, because 2 regions, 3 color components, and 13 + 5 types of features were used. The total number of features including Section 2.3.1 and 2.3.2 is 159.

It is ideal to calculate GLCM and GLRLM using all pixels on the image as the target pixel; however, these methods require a large amount of calculation. We therefore calculate for 7 × 7 pixels regions by 7 pixels skipping, calculate for 21 × 21 pixels regions by 21 pixels skipping, and interpolate their skipped pixels by the Cubic Convolution Interpolation (CCI) method.

2.3.4. Detail of SVM parameters

SVM is a supervised learning method that maps feature quantities to hyperplanes so as to maximize margins and classifies features into two classes. As a method of mapping, several kernel functions such as linear function and RBF (Radial Basis Function) have been proposed. Identifications of the linear function and the RBF are given by equation (1) and (2), respectively.

$$D_{x,y} = \mathrm{sgn}\left\{\sum_{j=1}^{n}\left\{C_j \sum_{i=1}^{m}\left(W_{j,i}\, F_{x,y,i}\right)\right\} + b\right\} \quad (1)$$

$$D_{x,y} = \mathrm{sgn}\left\{\sum_{j=1}^{n}\left\{C_j \exp\left(-\gamma \sum_{i=1}^{m}\left(W_{j,i} - F_{x,y,i}\right)^2\right)\right\} + b\right\} \quad (2)$$

Where $D_{x,y}$ is an identification result of a pixel coordinate (x,y) on a target image, $F_{x,y,i}$ is a i-th (i=1...m) feature value of the pixel (x,y), $W_{j,i}$ is a support vector for i-th feature value, and n is the number of elements of the support vector. $W_{j,i}$, C_j, and b are acquired by

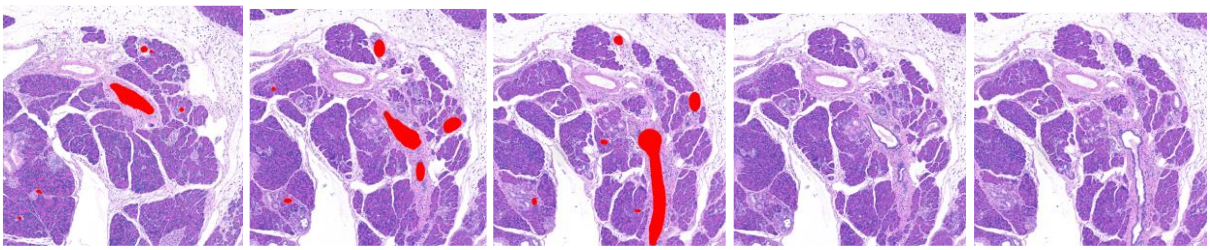

(a) 2nd slice. (b) 35-th slice. (c) 46-th slice. (d) Original of (b). (e) Original of (c).

Figure 4. (a)-(c) are training data filled pancreatic duct regions as red, and (d) and (e) are their original images.

Table 1. Conditions of experimental models.

Name	Feature value			SVM	
	Intensity	Shape	Texture	Function	C-param
MA (Model A)	use	use	all pixel	RBF	1000
MB (Model B)	use	use	all pixel	RBF	100
MC (Model C)	use	use	all pixel	RBF	10
MD (Model D)	use	use	all pixel	RBF	1
ME (Model E)	use	use	all pixel	linear	1
MF (Model F)	use	use	interpolation	linear	1
MG (Model G)	use	use	unused	linear	1
MH (Model H)	use	unused	unused	linear	1

machine learning of the SVM. γ is an input parameter, and we set $\gamma = 1 / m$.

The equation (1) can be decomposed into equations (3) and (4), and A_i of the equations (3) can be calculated in advance.

$$A_i = \sum_{j=1}^{n} \left(C_j W_{j,i} \right) \tag{3}$$

$$D_{x,y} = \mathrm{sgn}\left\{ \sum_{i=1}^{m} \left(A_i F_{x,y,i} \right) + b \right\} \tag{4}$$

The equation (4) consists of only a single loop; therefore the identification by the linear function is overwhelmingly faster than the RBF. However, the identification performance of the linear function is a lower than the one of the RBF, because the linear function cannot separate complex distribution of feature values. In the RBF, the learning model is represented more complicated by increasing a cost parameter (C-param); however it is likely to cause over learning. We therefore compare the calculation speed and the identification performance for 8 kinds of models shown in Table 1. Experimental results are described in Section 3.1.

2.4. Extraction of pancreatic duct regions

As in Section 2.3, pancreatic ductal regions are also extracted using shape feature values, texture feature values, and the machine learning of the SVM. As training data, we used 3 images shown in Figure 4 (a) to (c) whose pancreatic duct regions were manually filled as red. Figure 4 (d) and (e) are original images of Figure 4 (b) and (c), respectively. The original image of Figure 4 (a) is Figure 2 (a).

Our method of Section 2.3 use texture information; however the inside of the pancreatic duct is hollow and few texture information. We therefore do post-processing as follows.

(1) Pancreatic duct candidate regions identified by the SVM in Section 2.3 are labeled, fill in the labels, and labels of area under than 50 pixels are erase for noise removal.

(2) By calculating logical products of the candidate regions (binary images) of (1) between a slide and next slide, connections between the slide are calculated. By following this link, 3D labeling is implemented.

(3) By extracting labels of large volume in (2), pancreatic duct regions are extracted.

2.5. 3D reconstruction

3D reconstruction was performed by using a volume rendering software (Intage Realia Professional, CYBERNET SYSTEMS CO., LTD). If a pixel was identified as both the collagen fiber region and the pancreatic duct region, its pixel was set as the pancreatic duct region.

3. RESULTS AND DISCUSSION

3.1. Experimental method

HE stained slice images of 899 KPC mice were prepared according to the method described in Section 2.1, and the alignment was performed by the method described in Section 2.2. Afterward, “ROI 1” and “ROI 2” in Figure 1 were cut out, and the SVM for the fiber extraction described in Section 2.3 was carried out using the Figure. 3 (c) which is a partial region of “ROI 1”. Section 3.2 shows results of evaluating the processing time of the SVM, and Section 3.3 shows results of evaluating the accuracy of the SVM.

Similarly, the SVM for the pancreatic ductal region extraction was performed by using the method in

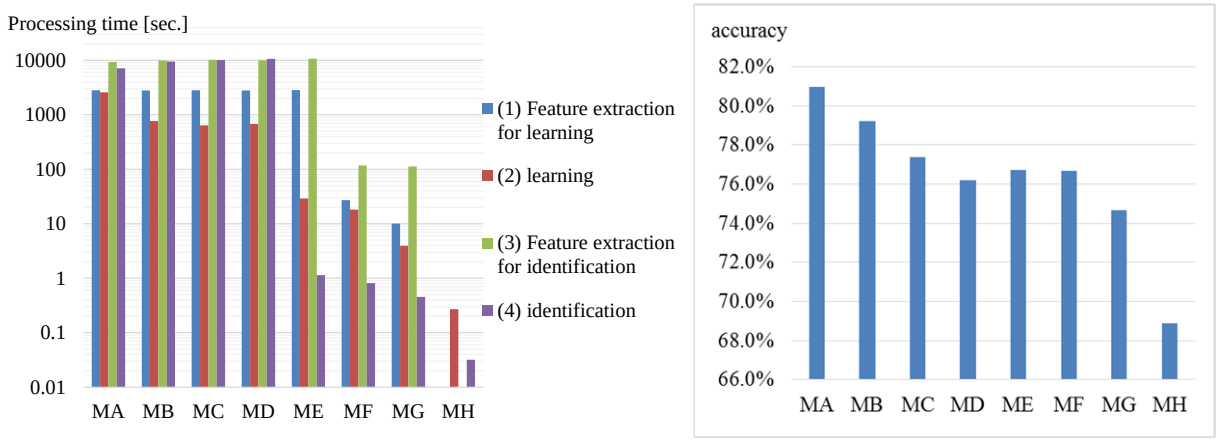

(a) Processing time of 8 models. The vertical axis is a log scale. (b) Accuracy of 8 models.

Figure 5. Comparison of processing time and accuracy of fiber region extraction experiment.

Section 2.4 and using Figure 4 (a) to (c) which are partial regions on "ROI 1". Afterward, we extracted fiber regions and pancreatic duct regions on "ROI 1" and "ROI 2" using the learned model. The extraction results and the 3D rendering results are shown in Section 3.4.

In all the experiments in this paper, the following hardware and software were used.

1) OS: Windows 8.1
2) CPU: Intel Core i7-4820K, 3.70GHz
3) RAM: 32.0GB
4) Integrated Development Environment: Microsoft Visual C++ 2010
5) SVM library: LibSVM and Liblinear [6]
6) Library: Intel OpenCV 2.4.2

3.2. Comparison of processing time for extracting the fiber region

Using the training data of Figure 3 (c), we performed the machine learning of the SVM to extract the collagen fiber regions for every 8 models (MA - MH) described in Section 2.3. In this section, we compare processing times required for machine learning when only one CPU is used (GPU or multitasking are not used).

Blue bars in Figure 5 (a) are processing times required for feature extraction for machine learning whose input data is Figure 3 (c) whose image size is 512 × 512 pixels. Red bars are processing times required for machine learning after the feature extraction. In both cases, vertical axes were displaying processing times on a logarithmic scale. Comparing blue bars, all models from MA to ME showed high values of about 2,800 seconds; however, MF showed low values of about 45 seconds. MF is a method in which the number of texture calculations is reduced by interpolation, and it was greatly shorten the processing time. Comparing red bars, MA was 2,582 second, and from MB to MD were about 700 second; however, ME was 29 second. This means the linear model takes much less time to learn than RBF.

Pathological image size is huge, and the processing time for identification is more important than the processing time for learning. The numbers of support vectors *n* for MA, MB, MC, and MD became 21,303, 22,920, 24,410, and 25,945, respectively, and it is expected that the identification times of ME and MF will be about 1 / 20,000 of ones of MA to MD. We therefore measured processing times required for the identification using the ROI of Figure 2 (a) whose image size is 1,000 × 1,000 pixels.

Green bars in Figure 5 (a) are processing times required for feature extraction for the identification, and purple bars are processing times required for the identification after the feature extraction. They showed the same tendency as blue and red bars. Comparing the purple bars, identification times of ME and MF became about ten-thousandth of ones of MA to MD, and approximately matched the theory. Comparing the total time required for identification, it takes about 3 to 6 hours for models of MA to ME, whereas MF and MG required about 2 minutes and MH was less than 0.1 seconds. The size of the whole image shown in Figure 1 is approximately 15,000 × 9,000 pixels, which is 135 times larger than the ROI calculated in this experiment. Therefore, to calculate one whole image, it takes several weeks in MA, whereas MF only requires 4 or 5 hours.

3.3. Comparison of accuracy for extracting the fiber region

Using the training data of Figure 3 (c) as in Section 3.2, we experimented to compare the extracting accuracy of the fiber region using 5-fold cross-validation of the SVM. Figure 5 (b) is the experimental result for 8 models described in Section 2.3.

	Slice number	(A) Original Image	(B) Result of MA	(C) Result of MF	(D) Result of MH
ROI 1	2	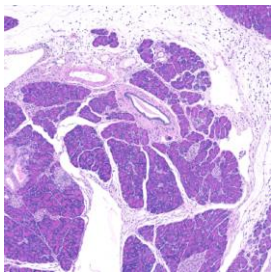 (1A) *1	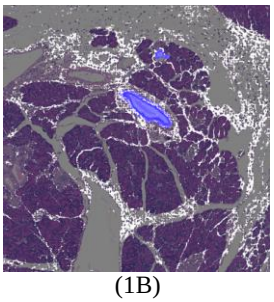 (1B)	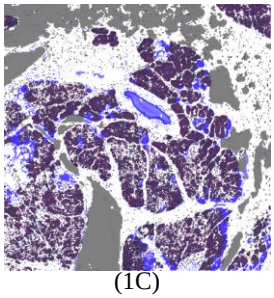 (1C)	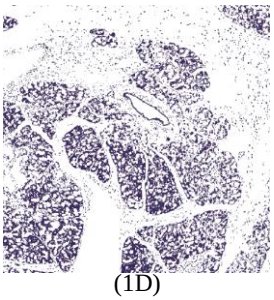 (1D)
	35	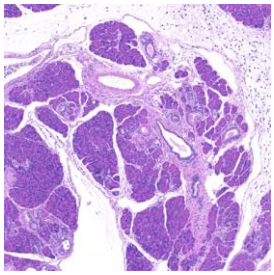 (2A) *1	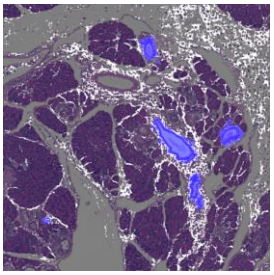 (2B)	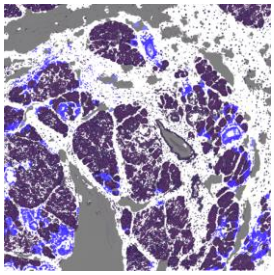 (2C)	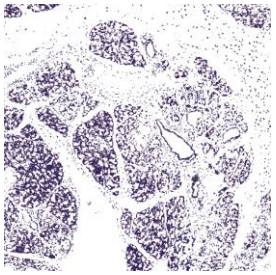 (2D)
	55	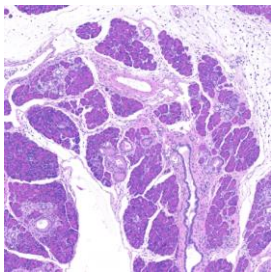 (3A)	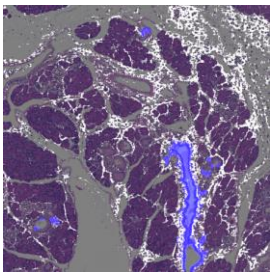 (3B)	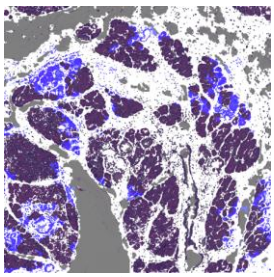 (3C)	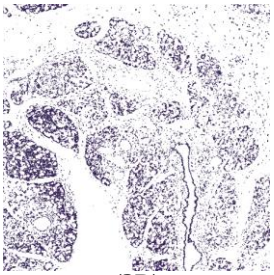 (3D)
ROI 2	2	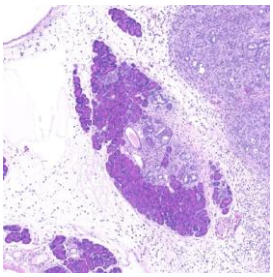 (4A)	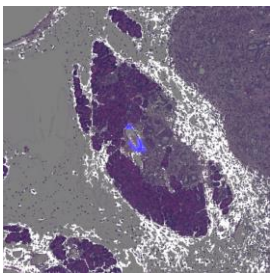 (4B)	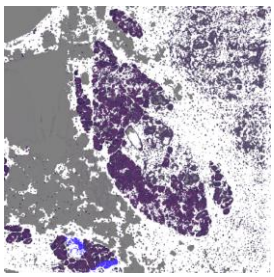 (4C)	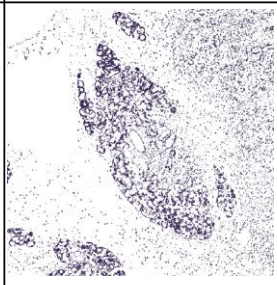 (4D)
	35	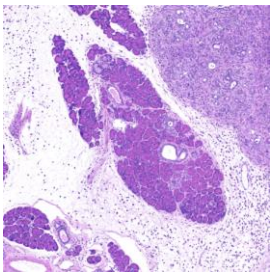 (5A)	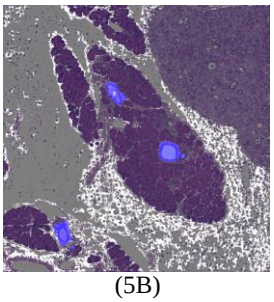 (5B)	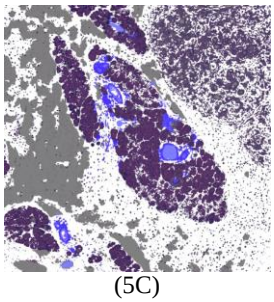 (5C)	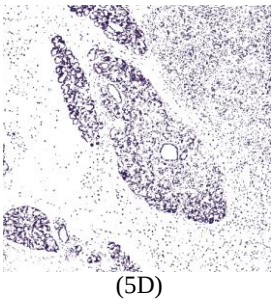 (5D)

Images of *1 were also used for learning of pancreatic ductal regions as shown in Figure 4.

Figure 6. Extracting results of the collagen fiber regions (white color) and pancreatic duct regions (blue color).

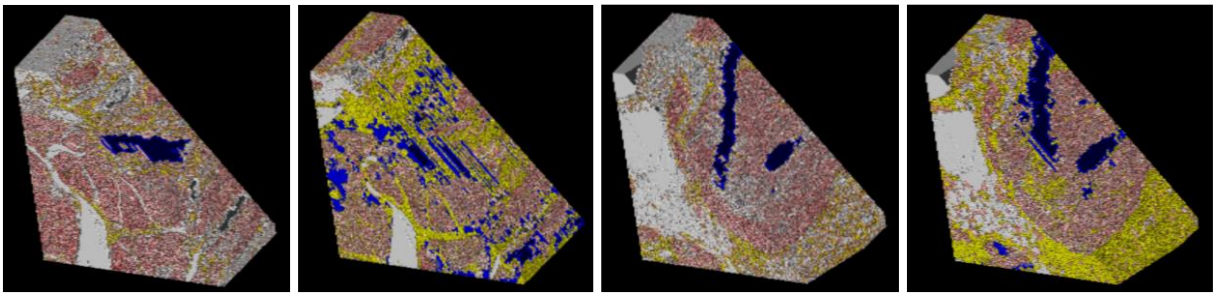

(a) "ROI 1" by MA. (b) "ROI 1" by MF. (c) "ROI 2" by MA. (d) "ROI 2" by MF.

Figure 7. 3D reconstruction results.

As shown in Figure 5 (b), since the accuracy of MG was higher than MH, shape feature values proposed in Section 2.3.2 were effective. Likewise, since the accuracy of MF was higher than MG, texture feature values proposed in Section 2.3.3 were also effective. The difference in accuracy between ME and MF is small. This result shows that the interpolation method described in Section 2.3.3 is less likely to degrade accuracy. On the other hand, the difference of the accuracy between ME and MA is a big. This result suggests that the use of a linear function may be a factor in reducing accuracy.

3.4. Comparison of 2D and 3D images of fiber and pancreatic duct regions extraction experiment

MA was the most accurate result in Section 3.3. MH was the fastest processing result in Section 3.2. In addition, MF was the model with moderate accuracy and speed of processing. We therefore identified the collagen fiber and the pancreatic duct regions using 3 models (MA, MF, and MH). The column (A) in Figure 6 represents original images, and columns (B), (C), and (D) represents the identification result images of MA, MF, and MH, respectively. The white color pixels on their images represents the collagen fiber region and the blue color pixels represents the pancreatic duct region. The first to third rows in Figure 6 show the identification results of "ROI 1", the fourth and fifth rows show the identification results of "ROI 2".

Results of 3D reconstruction by the method described in Section 2.5 is shown in Figure 7. Figure 7 (a) and (b) respectively show 3D reconstruction result images of MA and MF of "ROI 1", and Figure 7 (c) and (d) respectively show ones of MA and MF of "ROI 2". These were drawn oblique sections in perspective projection view. Yellow color in the figure represents the fiber region, and blue color represents the pancreatic ductal region.

In MA of column (B) in Figure 6, both of the pancreatic duct region and the fiber region are mostly successful in identification.

In MF of column (C), although fiber regions were roughly identified, their regions were widely identified. This matter is a possibility to improve by parameter adjustment. The pancreatic ductal regions of MF were a lot of identification failures although some were successful. Comparing MA and MF in Figure 7, there is no big difference in blue position between (c) and (d); however, there is a difference in blue position between (a) and (b). These results indicate that identifications of the pancreatic duct structure almost succeeded in "ROI 2", but failed in "ROI 1".

In MH of column (D) in Figure 6, pancreatic ductal regions were not identified and all the bright regions (include not only collagen fiber regions but also non-tissue regions and cytoplasm regions) were identified as collagen fiber regions.

Shape feature values proposed in Section 2.3.2 and texture feature values proposed in Section 2.3.3 were effective since results of MF was better than results of MH. On the other hand, there is a possibility that the linear kernel function modified for speeding up the processing were reduced the accuracy since results of MF were worse than results of MA. In order to solve the matter, we will study other feature values or learning models that can perform high speed processing.

4. CONCLUSIONS

In this study, we aimed to extract 3D structures of pancreatic duct and collagen fiber region from HE stained pathological images of pancreatic serial sections of KPC mouse, and performed intensities correction, alignment between sections, extraction of collagen fiber regions, and extraction of pancreatic duct regions for 3D model reconstruction. The alignment was performed by template matching using NCC method and extractions of both regions were used the machine learning by SVM. As feature values for SVM, we used shape feature and texture feature values. Shape feature values are composed of areas and circularities of regions obtained by binarization and labeling. Texture feature values are composed of co-occurrence matrix feature values and run-length matrix feature values. The effectiveness of these feature values was verified experimentally.

In our experiment, we compared the processing time and accuracy of high-precision model MA (using

all feature values and RBF kernel), high-speed model MH (using only intensities as feature values and linear kernel function), and intermediate model MF (using interpolation feature values and linear kernel function). As a result, MA successfully identified fiber and pancreatic duct regions; however, it took about 4 hours to calculate a ROI of 1,000 × 1,000 pixels using 1 CPU. On the other hand, MH was processed in less than 1 second; however, it failed to identify them. MF was able to identify ROI in about 2 minutes; however the accuracy of identification was slightly poor.

In the future, we will study other feature values or learning models that can perform high speed processing in order to improve the MF. We will also recognize malignant tumor regions using immunostaining with Ki67 antibody, and fuse with CT and MRI.

ACKNOWLEDGEMENT

This work was supported by MEXT Grant-in-Aid for Scientific Research on Innovative Areas, Saitama Medical University Internal Grant 26-B-1-09, SMU-FHMC Grant 25-019, and SMU-FHMC Grant 24-018.

REFERENCES

[1] Y. Song, D. Treanor, A. J. Bulpitt, D. R. Magee, "3D reconstruction of multiple stained histology images", J. Pathol. Inform., vol.4, no.7, Mar. 2013.

[2] K. Norton, S. Namazi, N. Barnard, M. Fujibayashi, G. Bhanot, S. Ganesan, H. Iyatomi, K. Ogawa, and T. Shinbrot, "Automated Reconstruction Algorithm for Identification of 3D Architectures of Cribriform Ductal Carcinoma In Situ", PLoS One, Vol.7, No.9, Sep. 2012.

[3] T. Y. Kim, H. J. Choi, H. G. Hwang, H. K. Choi, "Three-dimensional Texture Analysis of Renal Cell Carcinoma Cell Nuclei for Computerized Automatic Grading", J. Med. Syst. vol.34, no.4, pp.709-716, Aug. 2010.

[4] A. Shimizu, I. Hasegawa, N. Kobayashi, H. Shono, S. Nawano, I. Sato, H. Komagata, M. Ishikawa, K. Shinoda, "Fundamental Technologies for Integration of Multiscale Spatiotemporal Morphology in Multidisciplinary Computational Anatomy", The 2nd International Symposium on Multidisciplinary Computational Anatomy, Feb. 2016.

[5] C. Cortes and V. Vapnik, "Support-vector networks", Mach. Learn., vol.20, pp.273-297, 1995.

[6] Chang, C. C., Lin, C. J. "LIBSVM: A library for support vector machines", ACM Transactions on Intelligent Systems and Technology, Vol.2, No.3, pp.1-27, 2011.

[7] R. M. Haralick, K. Shanmugam, and I. Dinstein, "Texture feature for image classification," IEEE Trans. Syst. Man. Cybernet., vol.SMC-3, no.6, 1973.

[8] M. M. Galloway, "Texture analysis using gray level run lengths," Computer Graphics and Image Processing, vol.4, no.2, pp.172-179, 1975.